scientific reports

Check for updates

OPEN

Alfvén waves in the solar corona: resonance velocity, damping length, and charged particles acceleration by kinetic Alfvén waves

Syed Ayaz[1,6]✉, Gary P. Zank[1,6], Imran A. Khan[2,3,6], Gang Li[4] & Yeimy J. Rivera[5]

Recent advances in heliospheric exploration spurred by NASA's Parker Solar Probe (PSP) mission require a deeper understanding of the intricate dynamics of the solar corona and wind. This study provides a detailed examination of kinetic Alfvén waves (KAWs) within the $0-10$ R_{Sun} range, a region only briefly explored in future PSP passages. Employing the framework of kinetic plasma theory and incorporating a non-thermal Cairns velocity distribution, we investigate the impact of the non-thermal index parameter Λ on the resultant resonance velocity v_{res}. The results reveal a notable change in the distance (R_{Sun}) over which the particles transport energy and the magnitude of resonance velocity for $\Lambda > 0$. We also derive the perpendicular resonance velocity $v_{res\perp}$ and the group velocity v_g expressions of particles and KAWs, respectively. We find that $v_{res\perp}$ and the normalized group velocity v_g/v_A are significantly influenced by Λ. In contrast to the resonance speed and group velocity, the damping length L_D of KAWs is evaluated for different parameters. We find that KAWs experience accelerated damping and exhibit an increased damping length for $\Lambda > 0$. We evaluate KAWs by the influence of the magnetic field, variation in height relative to the solar radius R_{Sun}, and the electron-to-ion temperature ratio T_e/T_i. Collectively, these findings illustrate that KAWs not only are important for heating processes but also accelerate charged particles across considerable distances within the solar corona and solar wind regions. The analytical insights gleaned from this study find practical application in understanding wave phenomena in the solar and heliospheric regimes, particularly exploring the role of non-thermal particles in observed heating processes.

The solar wind, a continuous stream of fully ionized gas from the solar corona, plays a pivotal role in space physics[1,2]. Within the intricate tapestry of waves permeating the solar corona, solar wind, and various astrophysical environments, Alfvén waves stand out due to their significant influence on energy transfer mechanisms[3,4]. First proposed by Hannes Alfvén[5], these waves are crucial for the transport, acceleration, and heating of particles not only in space plasmas but also in laboratory plasma such as in fusion reactors[6,7]. Hasegawa and Chen[8] introduced these waves in the kinetic limit (also called kinetic Alfvén waves (KAWs)), a concept incorporating gyroradius corrections. More recently, KAWs have been studied by Khan et al.[9] in the solar corona and their role in energy transport and heating processes. KAWs, characterized by their ability to transfer substantial energy as heat during wave-particle interactions, are vital in understanding solar coronal dynamics[9–11]. Very recently, Rivera et al.[12] investigated the heating and acceleration of solar wind plasma as it moves from the outer edge of the solar corona to the inner heliosphere, supported by observations from the PSP and Solar Orbiter. The study shows that large-amplitude Alfvén waves contribute significantly to both plasma heating and acceleration. This observation can be linked to KAWs, which play a central role in transferring energy through wave-particle interactions, heating the plasma, and accelerating charged particles in the solar wind and solar corona.

[1]Department of Space Science and CSPAR, University of Alabama in Huntsville, Huntsville, AL 35899, USA. [2]Department of Space Sciences, Institute of Space Technology, Islamabad 44000, Pakistan. [3]Space and Astrophysics Research Lab (SARL), National Center of GIS and Space Applications (NCGSA), Islamabad 44000, Pakistan. [4]General Linear Space Plasma Lab LLC, Foster City, CA 94404, USA. [5]Center for Astrophysics, Harvard and Smithsonian, Cambridge, MA 02138, USA. [6]These authors contributed equally: Syed Ayaz , Gary P. Zank and Imran A. Khan . ✉email: sa0173@uah.edu; syedayaz263@gmail.com

The scientific interest in KAWs is driven by their essential role in various plasma phenomena, including their proposed function as an energy source for planetary auroras[13,14] and space weather-induced atmospheric escape[15]. Additionally, KAWs are key to space and astrophysical turbulence[16], potentially addressing the plasma heating mystery in the solar corona, solar wind, magnetospheres, and the interstellar medium[17]. These waves are noted for their rapid damping and efficient energy transfer to plasma particles. Temerin et al.[18] presented the first evidence of small-scale KAWs within the plasma sheet and plasma sheet boundary layer (PSBL). These waves potentially play a crucial role in the local heating of the plasma sheet and may generate earthward-moving, magnetic field-aligned electron beams and transversely heated ions. KAWs have been extensively studied by several researchers[9,17,19–21] (for details, see these references and references therein).

Recent advances through missions like Magnetospheric Multiscale (MMS), Cluster, and the PSP have opened up exciting possibilities for understanding our solar atmosphere[22–26]. One goal of these missions is to uncover how energy behaves in weakly collisional plasmas and how electrons and ions are energized[27]. One needs to understand the coupling of perturbed electromagnetic fields, temperature, density, and the overall behavior of individual charged species. Of particular importance is the knowledge of perturbed Electromagnetic fields and the Poynting flux of KAWs[28], we found that KAWs are responsible for energizing the charged particles through Landau resonance. Moreover, we studied the total power transfer rate of KAWs in the solar flux tube loops, approximating how KAWs transport power over spatial scales modified with increased non-thermal parameters. The study provides a comprehensive description of the heating processes of KAWs in the solar corona. However, other interesting phenomena remain, such as the resonance velocity of particles after Landau damping. The characteristic damping length, which estimates the distance over which waves transport energy, is also actively debated. Building on the work of Fahr and Shizgal[29], Schwenn[30], and Marsch[31], we use the Vlasov-Maxwell model and a kinetic plasma theory approach to investigate the group/resonance velocity and damping length of KAWs. This exploration elucidates KAWs' role in the solar corona and their connection with suprathermal ions and electrons. For a broader context, recommended readings include Benz[32] and Aschwanden[33], as well as the textbook by Aschwanden[34].

Within the context of current theories of the turbulent heating of the solar corona[35–37], magnetic energy is cascaded through the inertial range from large (energy-containing) to small scales, where it is assumed to dissipate and heat the plasma. Both the Alfvén wave/turbulence model[35] and the magnetic (nonlinear) turbulence model[36] assume that the dissipation occurs at high perpendicular wavenumber ($k_\perp$) values, in the kinetic regime, most likely via highly oblique KAWs. They have been postulated to be responsible for the highly perpendicular heating observed in the solar wind and corona[38–40]. The observations of slow Alfvénic solar wind emerging from low-latitude coronal holes, as described recently by Bale et al.[41], highlight the role of Alfvénic turbulence and enhanced Poynting flux in driving plasma heating and particle acceleration. Kasper et al.[42] discussed how Alfvén waves and structured velocity spikes in the solar wind contribute to energy transport and acceleration processes at about 35 R_{Sun}. These observations suggest that Alfvénic fluctuations play a crucial role in plasma heating and angular momentum loss. These findings align with our investigation of KAWs, with the focus on charged particle acceleration and heating through wave-particle interactions.

We focus on the heating and acceleration processes linked to KAWs in the solar atmosphere, where kinetic plasma physics is necessary to describe the behavior of ionized particles. Space-borne spectrometers measure particle composition and velocity distribution functions[31]. In a realistic plasma system, the charged particle distributions are not typically Maxwellian, and in general, the system is out of thermal equilibrium. To model such plasma particles, the literature employs various velocity distributions and relies on Vlasov/Boltzmann kinetic plasma theory to explore KAWs[9,20,21,43–45]. More recently, Huo, Du, and Guo[46] studied the temperature anisotropic KAWs in a Kappa-Maxwellian distribution, findings that the dispersion relation and damping rate of KAWs are modified with the variations in temperature anisotropy and the index parameter κ.

This paper uses the Cairns-distribution function, a novel approach first introduced by Cairns et al.[47], which has yet to be extensively explored in the literature. This nonthermal velocity distribution models the population of energetic particles observed in space plasmas by the Viking[48] and Freja[49] satellites. The Cairns distribution is characterized by its unique wing-like structures (Fig. 1), distinguishing it from other power-law distributions. The non-thermal index Λ within this distribution is a critical parameter, influencing the non-thermal characteristics of the system. In space plasma physics, the Kappa distribution[50] is widely accepted and frequently used. However, a comparison of the plots of both distributions reveals distinct differences: the Kappa distribution flattens and generates tails[51], whereas the Cairns distribution shows multiple shoulders (Fig. 1, left panel) in addition to tails (right panel).

Zank et al.[52] developed a model to explore the microstructure of the heliospheric termination shock and its impact on energetic neutral atom observations. In their model, they approximated proton distribution functions for the inner heliosheath, which closely resembles the Cairns distribution. When comparing the two, the Cairns distribution seems to describe two or three populations of charged particles that are not in thermal or collisional equilibrium. Zank et al.'s model proposes a superposition of three distinct populations: thermal protons from the solar wind, partially filled shells of energetic pickup ions (PUIs) and an even more energetic, non-gyrotropic population of pickup ions that were reflected at the shock and energized before being transmitted downstream. This mixture of non-equilibrated populations exhibits the features of the Cairns distribution. It would be interesting to test whether data from New Horizons could fit this combined PUIs distribution to a Cairns velocity distribution. Recently, Yang et al.[53] studied the effects of PUIs on shock front nonstationarity and energy dissipation at the heliospheric termination shocks, using 2D full particle simulations and comparing the results with *Voyager* 2 data. Their findings confirmed the structure proposed by Zank et al., validating their model. These studies provide crucial insights into the physical processes behind the Cairns distribution. It offers a helpful framework for understanding plasma dynamics in regions like the solar wind, ionosphere, and magnetosphere,

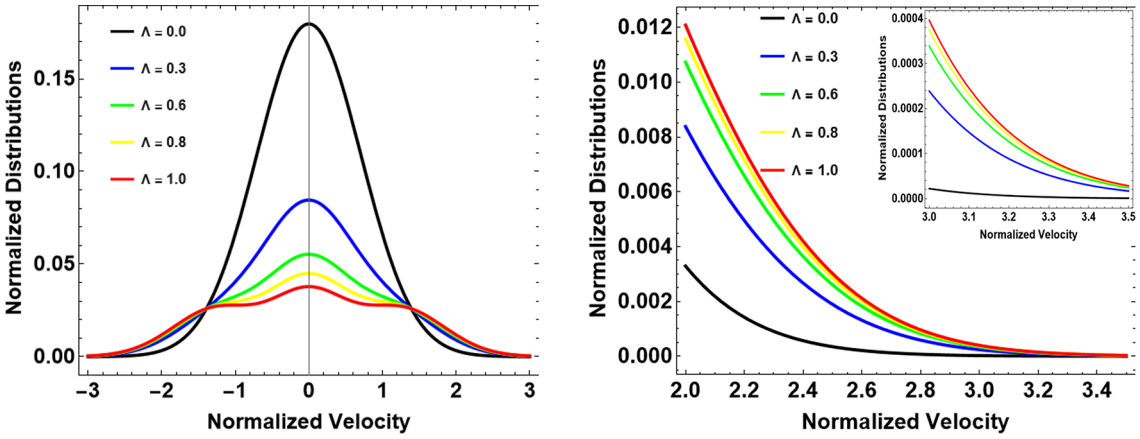

Fig. 1. Normalized distributions as a function of normalized velocity for different values of index parameter Λ . In the left panel, the horizontal and vertical axes are normalized as $\mathrm{v}/\mathrm{v}_{\mathrm{T}\alpha}$ and $\mathrm{v}_{\mathrm{T}\alpha}^3\mathrm{f}_{0\alpha}$, respectively. The right panel is the tails of the distribution functions for the same values of Λ with the inset showing more zoomed tails of the distributions from 3 to 3.5.

where non-thermal particles are frequently observed. Moreover, this non-Maxwellian distribution is invaluable for investigating theoretical models of nonthermal space plasmas, as evidenced by numerous studies[54–58].

One of the key strengths of the Cairns distribution lies in its mathematical convenience, particularly in modeling the velocity distribution of non-thermal particles. Unlike other distributions, it can describe bump-on-tail features or non-monotonic shoulder-like behaviors[59], which are essential for understanding instabilities in space plasma environments. This makes the Cairns distribution highly useful for studying wave-particle interactions and plasma instabilities in the solar wind and magnetospheric plasmas. From a mathematical perspective, the Cairns distribution can be viewed as an approximation of the Kappa distribution. Specifically, when the Kappa distribution is expanded for small values of the parameter $\mathrm{v}^2/\kappa\mathrm{v}_{\mathrm{T}}^2 \ll 1$, we arrive at a form similar to the Cairns distribution. The expansion looks like this:

$$f(\mathrm{v}) \propto \left[1 + c_1\mathrm{v}^2/\mathrm{v}_{\mathrm{T}}^2 + c_2\mathrm{v}^4/\mathrm{v}_{\mathrm{T}}^4 + ...\right] \times e^{-\mathrm{v}^2/\mathrm{v}_{\mathrm{T}}^2},$$

where $c_1 = -1/\kappa$ and $c_2 = 1/2\kappa$. When $c_1 = 0$, the original Cairns distribution (Eq. (1)) is recovered, as shown by Hau and Fu[60] and Wang and Hau[61]. This mathematical insight helps bridge the gap between the Cairns and Kappa distributions, offering some theoretical basis for its application. This distribution is extensively reported in numerous papers in combination with the Vasyliunas distribution, also called the Vasyliunas-Cairns.

Some regions in space exhibit particle distributions resembling the Cairns distribution. For instance, Retterer, Chang, and Jasperse[62] studied ion acceleration in the suprauroral region, with simulation results that align closely with the Cairns-distribution function. Recently, Livadiotis et al.[63] investigated the flux and energy spectrum of energetic neutral atoms using PUIs[64] and Kappa-distributions. Their analysis revealed that the spherical shell structures of the PUI distribution form shoulder-like features under the influence of the Kappa distribution. Specifically, the combination of Maxwellian and PUI distributions closely resembles the structures found in the Cairns distribution function. This is a key reason for using the Cairns distribution in our work. We anticipate that other regions may also exhibit particle distributions that align well with the Cairns distribution. Ongoing research could soon identify more such areas.

In our recent work[28], we investigated the Poynting flux vector and the total power transfer rate by KAWs. However, the existing literature did not address aspects like the resonance particle velocities, group speed, and the characteristic damping length, particularly in a Cairns-distributed plasma. The purpose of this study is to address these issues. From the expression of the resonance velocity, we can explicitly see the velocity variations with distance. The group speed is also very important; it tells us how the energy flows. The damping length of KAWs provides insight into how far these waves and particles can transport energy before being damped. These aspects are mainly attributed to the KAW-induced heating and charged particle acceleration. Specifically, we address how KAWs induce heating and acceleration in charged particles within the solar corona. A key aspect of our investigation involves understanding the influence of non-thermal particles Λ together with variations in magnetic field **B** and the electron-to-ion temperature $(\mathrm{T_e}/\mathrm{T_i})$ ratio on the group and resonance velocity through heating rate, and damping length of KAWs.

The manuscript's structure is as follows: Section "Basic equations" delineates the basic equations supporting our analytical model. Sections "Resonance velocity of particles" and "The characteristic damping length of KAWs" investigate the generalized resonance velocity and damping length expressions of KAWs. Section "Result and discussion" discusses the results, and finally, Section "Concluding remarks" presents concluding remarks.

Basic equations

To derive the governing equations, we assume a collisionless, homogeneous, and low-beta electron-ion plasma in which the Alfvén waves travel in the kinetic limits, i.e., $m_e/m_i \ll \beta \ll 1$ (where $\beta = \mathrm{c_s}^2/\mathrm{v_A}^2 = 4\pi n_0 \mathrm{T}_s/\mathrm{B}_0^2 \ll 1$). Moreover, the plasma possesses non-thermal features. To model such a plasma, we use the Cairns distribution which can be expressed as

$$f_{0\alpha} = \frac{1}{(1+\Lambda\frac{15}{4})\pi^{3/2}\mathrm{v}_{\mathrm{T}\alpha}^3}\left(1+\Lambda\frac{\mathrm{v}^4}{\mathrm{v}_{\mathrm{T}\alpha}^4}\right)e^{-\frac{\mathrm{v}^2}{\mathrm{v}_{\mathrm{T}\alpha}^2}}, \tag{1}$$

where $\mathrm{v}_{\mathrm{T}\alpha} = (2\mathrm{T}_\alpha/m_\alpha)^{1/2}$ is the thermal velocity with temperature (T_α) and mass (m_α) of the $\alpha-$species (α denotes ions or electrons). $\Lambda(\geq 0)$ is a spectral index parameter controlling the non-thermal characteristics of the plasma system. In the work of Cairns et al.[47], a one-dimensional distribution was expressed which is slightly different from Eq. (1), but in the current study, we need a three-dimensional distribution function defined by Eq. (1). The 3D form of the Cairns-distribution function Eq. (1) is obtained by considering temperature anisotropy in the distribution mentioned in Khan et al.[65]. Using kinetic theory, many important quantities can be calculated using (1), for example, following the procedure mentioned by Zank[66], the thermal conductive flux q_i in the Cairns-distributed plasma turns out to be

$$q_i = -\frac{(1+\Lambda)}{(1+\frac{15\Lambda}{4})}\frac{5}{2}\frac{k_B^2\mathrm{T}}{m\nu}\frac{\partial \mathrm{T}}{\partial x_i},$$

where ν represents the scattering frequency and all other symbols have their usual meaning. One can directly recover Maxwellian results when $\Lambda = 0$.

For convenience (as shown in Fig. 2), the system's geometry is such that the wave is emitted from a source at position $z = 0$ and propagates in the $x - z$ plane. Assuming that the plasma supports a low-frequency wave which means that the wave frequency is smaller than the ion gyro-frequency i.e., $\omega < \Omega_i$. Furthermore, the wave propagates obliquely to the ambient magnetic field B_0 which points along the $z-$axis. The magnetic field of the wave is along $y-$axis and the electric field **E** of the waves lies in the $x - z$ plane. We evaluate KAWs in the solar flux tube loop and the schematic Fig. 2 represents the fitted geometry of obliquely propagating KAWs in the flux tube.

Employing the Vlasov-Maxwell set of equations, the dispersion relation for such a plasma configuration takes the form[67,68]:

$$\begin{pmatrix} \epsilon_{xx} - \frac{k_z^2c^2}{\omega^2} & \frac{k_xk_zc^2}{\omega^2} \\ \frac{k_xk_zc^2}{\omega^2} & \epsilon_{zz} - \frac{k_z^2c^2}{\omega^2} \end{pmatrix} \begin{pmatrix} \mathrm{E_x} \\ \mathrm{E_z} \end{pmatrix} = 0. \tag{2}$$

Here, ω is assumed complex $\omega = \omega_r + i\omega_i$ with $\omega_i \ll \omega_r$, where *r* and *i* represent the real and imaginary parts, respectively. ϵ_{xx} and ϵ_{zz} are the permittivity tensors, k_z and k_x are the corresponding parallel and perpendicular wave vectors to the mean magnetic field B_0, and *c* the speed of light.

The two permittivity tensor components (ϵ_{xx} and ϵ_{zz}) are

$$\epsilon_{xx} = 1 + \sum_\alpha \frac{\omega_{p\alpha}^2}{\omega}\int d^3v \sum_{n=-\infty}^{\infty} \frac{n^2}{\zeta^2}\frac{v_x J_n^2(\zeta)}{(\omega - k_z v_z - n\Omega_\alpha)}\frac{\partial f_{0\alpha}}{\partial v_x}, \tag{3}$$

and

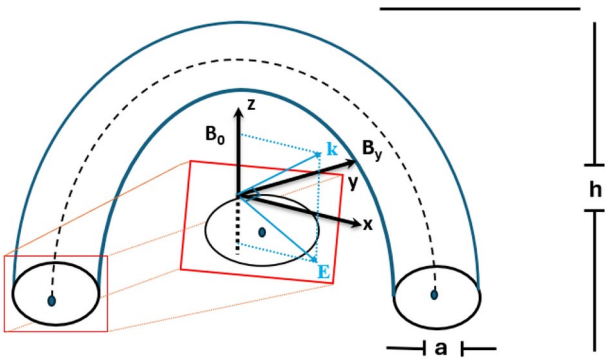

Fig. 2. Geometry of obliquely propagating Alfvén waves. The schematic diagram indicates the fitted geometry of KAWs in a solar flux tube loop of height h and a circular cross-section of radius *a*.

$$\epsilon_{zz} = 1 + \sum_{\alpha} \frac{\omega_{p\alpha}^2}{\omega} \int d^3v \sum_{n=-\infty}^{\infty} \frac{J_n^2(\zeta)}{(\omega - k_z v_z - n\Omega_\alpha)} \frac{v_z^2}{v_x} \frac{\partial f_{0\alpha}}{\partial v_x}, \tag{4}$$

and $\omega_{p\alpha} = (4\pi n_0 e^2/m_\alpha)^{1/2}$ is the plasma-frequency, $\Omega_\alpha = qB_0/m_\alpha c$ is the gyro-frequency, and $J_n^2(\zeta)$ is the Bessel function with argument $\zeta = k_x v_x/\Omega$, respectively. Upon using $f_{0\alpha}$ in Eqs. (3) and (4) and solving the parallel and perpendicular integrals, the two permittivity tensor expressions become[69,70],

$$\epsilon_{xx} = \frac{1}{(1+\Lambda\frac{15}{4})} \frac{\mathrm{c}^2}{\mathrm{v}_\mathrm{A}^2} \Big(1 - \frac{3}{4}k_x^2\rho_i^2 + \frac{\Lambda}{4}\Big), \tag{5}$$

and

$$\epsilon_{zz} = -\frac{1}{(1+\Lambda\frac{15}{4})} \Big(\frac{Z^{'}(\xi_e)}{2k_z^2\lambda_{\mathrm{De}}^2} + \frac{Z^{'}(\xi_i)}{2k_z^2\lambda_{\mathrm{Di}}^2}\Big). \tag{6}$$

Here $\mathrm{v_A} = \mathrm{B}_0/(4\pi n_0 m_i)^{1/2}$ is the Alfvén velocity, $\rho_i^2 (= \mathrm{v}_{\mathrm{Ti}}^2/2\Omega_i^2)$ is ion gyroradius, $\lambda_{\mathrm{De,i}} (= \mathrm{v_{Te,i}}/2\omega_{pe,i})$ is the electron/ion Debye length, and $Z^{'}(\xi_{e,i})$ is the derivative of the plasma dispersion function[71],

$$Z(\xi_{e,i}) = \frac{1}{\sqrt{\pi}} \int_{-\infty}^{\infty} \frac{e^{-s^2}}{(s - \xi_{e,i})} ds,$$

with argument $\xi_{e,i} = \omega/k_z \mathrm{v_{Te,i}}$.

Since we are dealing with the kinetic limits in which $\xi_e \ll 1$, the plasma dispersion function for electrons takes the form

$$Z^{'}(\xi_e) \approx -2(1 + i\xi_e\sqrt{\pi}e^{-\xi_e^2}).$$

Similarly the Z-function for ions ($\xi_i \gg 1$) becomes

$$Z^{'}(\xi_i) \approx (\xi_i^{-2} - 2i\xi_i\sqrt{\pi}e^{-\xi_i^2}).$$

Using the values of the Z-functions in Eq. (6) and substituting both Eqs. (5) and (6) back into Eq. (2) yield

$$\omega_r = k_z \mathrm{v_A} \left[\left(\frac{1 + \Lambda\frac{15}{4}}{1 + \frac{\Lambda}{4}} \right) \left(1 + \frac{3}{4}k_x^2\rho_i^2\right) + \frac{\mathrm{T_e}}{\mathrm{T_i}} k_x^2\rho_i^2 \Big(1 + \Lambda\frac{15}{4}\Big) \right]^{1/2}, \tag{7}$$

and

$$\omega_i = -\gamma k_z \mathrm{v_A}, \tag{8}$$

with

$$\gamma = \frac{\mathrm{v_A}}{\mathrm{v_{Tze}}} \frac{(1+\Lambda\frac{15}{4})}{2} \left[\frac{\mathrm{T_e}}{\mathrm{T_i}} k_x^2\rho_i^2 \left\{ 1 + \Big(\frac{\mathrm{T_e}}{\mathrm{T_i}}\Big)^{3/2} \sqrt{\frac{m_i}{m_e}} e^{-\xi_i^2} \right\} \right] \sqrt{\pi}. \tag{9}$$

Utilizing Eqs. (7)–(9), we obtain both the parallel and perpendicular components of the Poynting flux vector for KAWs[28]:

$$\mathrm{S_z}(z) = \mathrm{S_z}(0) exp(-2k_z\gamma C_0 z), \tag{10}$$

and

$$\mathrm{S_x}(z) = -\mathrm{S_z}(0) \Big(\frac{\mathrm{E_z}}{\mathrm{E_x}}\Big) exp(-2k_z\gamma C_0 z), \tag{11}$$

where $C_0 = \left(\frac{1+\frac{\Lambda}{4}}{1+\Lambda\frac{15}{4}}\right)^{1/2}$, $\mathrm{S_z}(0)$ represents the Poynting flux vector at location $z = 0$, and

$$\frac{\mathrm{E_z}}{\mathrm{E_x}} = \frac{k_z}{k_x} \Big[1 - \Big(1 - \frac{3}{4}k_\perp^2\rho_i^2 + \frac{\Lambda}{4}\Big) \Big\{ \Big(1 + \frac{3}{4}k_\perp^2\rho_i^2\Big) + \frac{\mathrm{T_e}}{\mathrm{T_i}} k_\perp^2\rho_i^2 \Big(1 + \frac{\Lambda}{4}\Big) \Big\} \Big];$$

see our recent work by Ayaz et al.[28].

Resonance velocity of particles

Following the general expression for the law of conservation of kinetic energy in terms of the Poynting flux[72],

$$\mathbf{S} = \frac{1}{2}\rho \mathrm{v}^3,$$

we find

$$\mathbf{v} = \left(\frac{2\mathbf{S}}{\rho}\right)^{1/3}. \tag{12}$$

Expression (12) represents the speed the particles gain after the wave-particle interaction as a result of the Landau resonance.

The particles that fulfill the resonance condition, i.e., interacting with the wave and, as a result, receiving energy from the wave, have a velocity that is equal to the sum of the particle's initial velocity (which is approximately equal to the wave phase velocity for the particles that resonate with the wave) and the additional velocity after gaining energy from the wave as it damps. The newly acquired velocity generally represents a significant increase, much like in a Tip-cat game where particles initially receive momentum from the wave and subsequently travel at a faster pace, therefore

$$\mathrm{v}_{\mathrm{res}} = \frac{\omega_r}{k_z} + \left(\frac{2\mathrm{S(x,z)}}{\rho}\right)^{1/3}, \tag{13}$$

Here, ρ is the mass density, and $\mathrm{v}_{\mathrm{res}}$ is the net velocity of resonance particles. The parallel component of the wave-vector k_z is because the wave mostly delivers energy along the magnetic field lines. By utilizing the previous analytical expressions (7) and (10) in Eq. (13), we obtain the normalized resonance or net velocity of the particles as

$$\frac{\mathrm{v}_{\mathrm{res}}}{\mathrm{v}_{\mathrm{A}}} = \left[\frac{1}{C_0^2}\left(1 + \frac{3}{4}k_x^2\rho_i^2\right) + \frac{\mathrm{T_e}}{\mathrm{T_i}}k_x^2\rho_i^2\right]^{1/2} + \frac{1}{\mathrm{v}_{\mathrm{A}}}\left(\frac{2\mathrm{S}z(0)exp(-2k_z\gamma C_0 z)}{\rho}\right)^{1/3}. \tag{14}$$

This expression quantifies the resonance velocity along the parallel direction. KAWs transport more energy in the parallel direction. In general, the perpendicular contribution has not been considered due to its relatively small contribution. However, KAWs in the solar coronal regions dissipate possibly in the perpendicular direction, for instance, for our chosen parameter, $k_x\rho_i \approx 0.01$ may be important. Doing the same algebra as earlier, using Eqs. (7) and (11) in Eq. (13) gives the normalized perpendicular resonance velocity as

$$\frac{\mathrm{v}_{\mathrm{res}\perp}}{\mathrm{v}_{\mathrm{A}}} = \left[\frac{1}{C_0^2}\left(1 + \frac{3}{4}k_x^2\rho_i^2\right) + \frac{\mathrm{T_e}}{\mathrm{T_i}}k_x^2\rho_i^2\right]^{1/2} + \frac{1}{\mathrm{v}_{\mathrm{A}}}\left(-\frac{\mathrm{E}_z}{\mathrm{E_x}}\frac{2\mathrm{S}_z(0)exp(-2k_z\gamma C_0 z)}{\rho}\right)^{1/3}. \tag{15}$$

The characteristic damping length of KAWs

The damping length of KAWs is given by[73]

$$\mathrm{L_D} = \frac{\mathrm{v_g}}{\omega_i}, \tag{16}$$

where $\mathrm{v_g}$ is the group velocity defined as:

$$\mathrm{v_g} = \sqrt{\left(\frac{\partial\omega_r}{\partial k_x}\right)^2 + \left(\frac{\partial\omega_r}{\partial k_z}\right)^2}. \tag{17}$$

On evaluating Eq. (7) and substituting those values in Eq. (17), we obtain the normalized group velocity as

$$\frac{\mathrm{v_g}}{\mathrm{v_A}} = \frac{\left[\frac{1}{C_0^2}(1 + \frac{3}{4}k_x^2\rho_i^2) + \frac{\mathrm{T_e}}{\mathrm{T_i}}k_x^2\rho_i^2\right] + \left[\frac{1}{C_0^2}(\frac{3}{4}k_xk_z\rho_i^2) + \frac{\mathrm{T_e}}{\mathrm{T_i}}k_zk_x^2\rho_i^2\right]}{\left[\frac{1}{C_0^2}(1 + \frac{3}{4}k_x^2\rho_i^2) + \frac{\mathrm{T_e}}{\mathrm{T_i}}k_x^2\rho_i^2\right]^{1/2}}. \tag{18}$$

Using Eqs. (18) and (8) in Eq. (16) yields

$$\mathrm{L_D} = -\frac{2\mathrm{v_{Te}}}{\mathrm{v_A}}\left\{\frac{\frac{1}{k_z}\left[\frac{1}{C_0^2}\left(1 + \frac{3}{4}k_x^2\rho_i^2\right) + \frac{\mathrm{T_e}}{\mathrm{T_i}}k_x^2\rho_i^2\right] + \left[\frac{1}{C_0^2}(\frac{3}{4}k_x\rho_i^2) + \frac{\mathrm{T_e}}{\mathrm{T_i}}k_x^2\rho_i^2\right]}{\left[\frac{1}{C_0^2}(1 + \frac{3}{4}k_x^2\rho_i^2) + \frac{\mathrm{T_e}}{\mathrm{T_i}}k_x^2\rho_i^2\right]^{1/2}\left(1 + 15\frac{\Lambda}{4}\right)\frac{\mathrm{T_e}}{\mathrm{T_i}}k_x^2\rho_i^2\left[1 + \sqrt{\frac{m_i}{m_e}}\left(\frac{\mathrm{T_e}}{\mathrm{T_i}}\right)^{3/2}exp(-\xi_i^2)\right]\sqrt{\pi}}\right\}. \tag{19}$$

Result and discussion

The following plasma parameters are appropriate to the solar wind and solar coronal regions[74–77]: temperature T $\sim 10^6$ Kelvin, the density n_0 is $(10^9 - 10^{11})$ cm^{-3}, the ambient magnetic field **B** is $(10 - 100)$ G, k_x/k_z $(\sim 100 - 115)$, and the plasma beta $\beta_p = 4\pi n_0 \mathrm{T}/\mathrm{B}_0^2 \ll 1$.

The normalized resonance velocity $\mathrm{v_{res}}$ of the particles in the parallel direction exhibits substantial sensitivity to the nonthermal parameter Λ, as illustrated in Fig. 3. We assessed $\mathrm{v_{res}}$ under various conditions. Initially, assuming a magnetic field strength **B** of 10 G and an electron-to-ion temperature ratio $\mathrm{T_e/T_i}$ of 0.1, the resultant net speed of the particles decay slower with increasing values of Λ, as shown in Fig. 3 (left panel). The particles transport energy and can heat the solar corona over extended distances (i.e., ~ 150 $\mathrm{R_{Sun}}$). Subsequently, with **B** set at 20 G but maintaining the same temperature ratio, an analogous decay rate is observed, as illustrated in Fig. 3, right panel. Notably, in both scenarios, it is evident that the particles' speed exhibits a more extensive energy propagation range when **B** is 10 G in comparison to **B** being 20 G. This discrepancy arises from the stronger wave-particle interactions prevailing in the 20 G magnetic field compared to the 10 G field, thereby facilitating increased wave travel distances ($\mathrm{R_{Sun}}$). Upon introducing a higher temperature ratio $(\mathrm{T_e/T_i} = 0.3)$, i.e., the inset in the left panel, for the same variation in Λ, illustrates that the particles now travel comparatively shorter distance (~ 30 $\mathrm{R_{Sun}}$) than in the preceding cases. The increased temperature ratio leads to a notable reduction in the particles' propagation range. This phenomenon is attributed to the stronger wave-particle resonance interactions influenced by temperature. Consequently, at elevated temperatures, $\mathrm{v_{res}}$ undergoes slower decay over shorter distances when a Cairns-distributed state describes the plasma. Conversely, in the suprathermal state, the wave's energy transfer to particles occurs over a limited range and propagates for a shorter distance. This intricate interplay between nonthermal parameters and temperature underscores the nuanced nature of wave-particle interactions in plasmas, possessing a non-Maxwellian energetic particle composition.

In the preceding investigation, we initially considered a flux ribbon height of h = 0.05 $\mathrm{R_{Sun}}$[78]. Subsequently, by increasing the height to h = 0.1 $\mathrm{R_{Sun}}$, the resonance velocity is explored under various conditions, specifically for different values of Λ. This analysis assumed magnetic field strengths of **B** = 10 G and **B** = 20 G while maintaining a constant temperature ratio of $\mathrm{T_e/T_i} = 0.1$, as illustrated in Fig. 4. Remarkably, an observable reduction in the transported particle's energy over distance is perceived in comparison to the h = 0.05 $\mathrm{R_{Sun}}$ scenario. Particularly noteworthy is the weak decay of resonance particles in Cairns-distributed plasmas when $\Lambda \geq 0$. This underscores the influence of nonthermal effects on the particle's velocity, with a distinct manifestation in the decay characteristics.

We also elucidated the normalized $\mathrm{v_{res}/v_A}$ for the case when $\mathrm{T_e/T_i} = 0.3$ (inset in the left panel). In this case, the energy transport by the particles is more limited, indicating that the wave-particle interactions are intensified in this parameter regime. Notably, for relatively longer distances i.e., beyond 8 $\mathrm{R_{Sun}}$, the disparity in particle velocity behavior between Cairns and Maxwellian distributed plasmas becomes less obvious. For larger temperature ratios, the particle velocity is less sensitive to the distribution function, suggesting a convergence of behavior over extended spatial scales. The interplay between nonthermal parameters, magnetic field strength, and temperature ratio illustrates the complicated nature of energy transfer by the particles in the solar corona.

Rivera et al.[12] conducted an insightful study using *in situ* measurements from the PSP and Solar Orbiter spacecraft to investigate the solar wind as it travels through the inner heliosphere. Their observations revealed significant plasma heating and acceleration between the outer corona and the region near Venus' orbit, driven by the presence of large amplitude Alfvén waves. Notably, they demonstrated that the damping and mechanical energy transfer from these waves are sufficient to power the fast solar wind's heating and acceleration in the inner

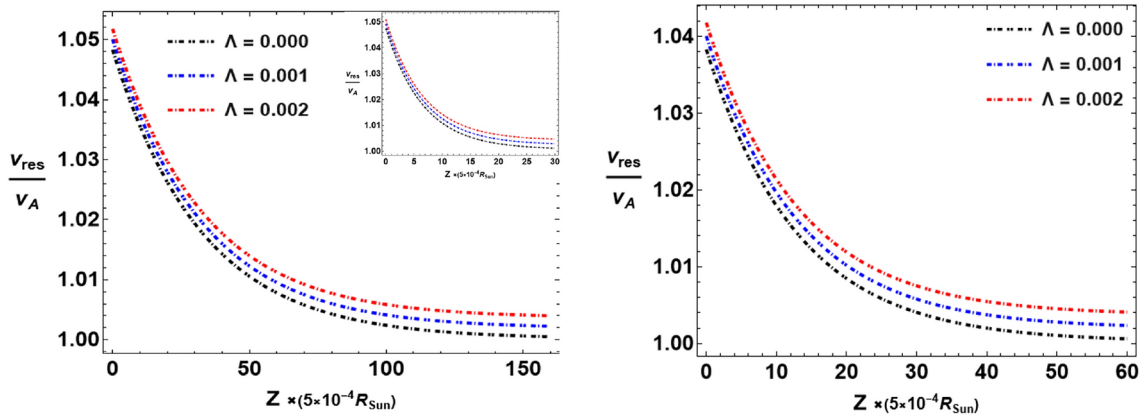

Fig. 3. Normalized resonance velocity $\mathrm{v_{res}/v_A}$ vs. normalized perpendicular distance $Z \times 0.0005$ $\mathrm{R_{Sun}}$ for different values of Λ. The plots are generated using Eq. (14) with the following parameter values: $k_x\rho_i = 0.06$, the normalized Poynting flux $\mathrm{S}_z(0) \sim \times 10^4$ W $\mathrm{m^{-2}}$, the electron mass density $\rho = m_e n$, $\rho_i \approx 2.58 \times 10^2$ cm, $k_x \approx 2.4 \times 10^{-4}$ $\mathrm{cm^{-1}}$, $k_z \approx 2.32 \times 10^{-6}$ $\mathrm{cm^{-1}}$, h = 0.05 $\mathrm{R_{Sun}}$, and the electron-to-ion temperature ratio $\mathrm{T_e/T_i} = 0.1$. The left panel is for **B** = 10 G and the right panel is for **B** = 20 G. The small inset in the left panel is for larger values of temperature i.e., $\mathrm{T_e/T_i} = 0.3$ with the same variation in Λ. In both cases, the net perpendicular resonance velocity is significantly influenced by different values of Λ.

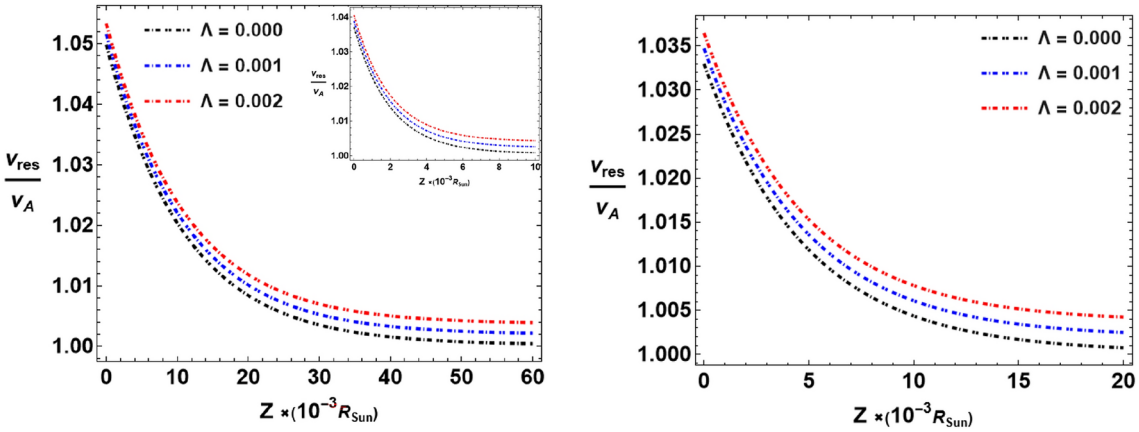

Fig. 4. Normalized resonance velocity $\mathrm{v_{res}/v_A}$ vs. normalized perpendicular distance $Z\times 0.001$ $\mathrm{R_{Sun}}$. The parameters are the same as those in Fig. 3 except h = 0.1 $\mathrm{R_{Sun}}$. In the left panel, **B** = 10 G and in the right panel, **B** = 20 G. Different values of Λ significantly influence the parallel resonance velocity. The inset shows how the larger values of electron-to-ion temperature ($\mathrm{T_e/T_i} = 0.3$) affect the resonance velocity for the given variation in Λ.

heliosphere. In our study, we compare our analytical results to those of Rivera et al.[12]. They reported an Alfvén speed of about $\mathrm{v_A} \approx 4.35 \times 10^7$ cm/s at a distance of 13.5 $\mathrm{R_{Sun}}$. To ensure consistency with their findings, we assumed a magnetic field strength of **B** = 10 - 20 G in our model. This yielded an Alfvén speed of approximately $\mathrm{v_A} \approx 3 \times 10^8$ cm/s, a value that is largely consistent with Rivera et al.'s results. The small discrepancy can be attributed to the different distances considered, as our model focused on a region closer to the Sun, between 0.05 and 0.1 $\mathrm{R_{Sun}}$.

Additionally, Rivera et al. reported a bulk proton speed of about $\mathrm{v}_\alpha \approx 3.96 \times 10^7$ cm/s at 13.5 $\mathrm{R_{Sun}}$. In contrast, our analysis of the resonance particle speed ($\mathrm{v_{res}/v_A}$) shows particles reaching speeds around 3.15×10^8 cm/s at 0.05 to 0.1 $\mathrm{R_{Sun}}$, as shown in Figs. 3 and 4. This suggests that while there are some differences in speed due to the varying distances considered, our results are overall well-aligned with Rivera et al., further supporting the role of KAWs in driving particle acceleration and heating in the solar corona.

For KAW scales, where $k_x \gg k_z$, the contribution of wave-particle interactions, Poynting flux, power rates, and energy transport in the perpendicular direction is very small. However, our investigation of KAWs in the solar corona addresses that even this minor contribution is also equally important[28]. Previous studies[67,79,80] have primarily focused on wave dynamics outside the solar corona, overlooking these subtle contributions. In our research, particularly for a warm plasma, we emphasize the significance of the perpendicular resonance velocity, even with their minor contributions. For the solar flux ribbon (shown in Fig. 2), the energy transfer in the perpendicular direction is crucial in defining the width of the solar flux loop tube. In this context, the normalized perpendicular wavenumber $k_x\rho_i$ is small but significant for particle energization. In the solar corona, a smaller $k_x\rho_i$ value (i.e., ~ 0.01 for our chosen parameters) plays a predominant role. This is the prime reason why we do not ignore the resonance velocity of particles in the perpendicular direction.

The normalized perpendicular resonance velocity ($\mathrm{v_{res\perp}}$) is plotted in Fig. 5, showing that it is larger in magnitude for a minor increment in Λ (> 0). The figures reveal that the perpendicular velocity notably heats the solar corona for a short distance ($\mathrm{R_{Sun}}$), e.g., ~ 7 $\mathrm{R_{Sun}}$, compared to the parallel resonance counterpart, as illustrated in Figs. 3 and 4. Intriguingly, under conditions where the temperature ratio is increased i.e., $\mathrm{T_e/T_i} = 0.3$ (see the inset in the left panel), the particles transport energy over a shorter distance ($\mathrm{R_{Sun}}$). Consequently, the disparity between Cairns and Maxwellian distributed plasmas diminishes as the distance increases, i.e., > 2 $\mathrm{R_{Sun}}$. This observation underscores the importance of temperature on wave-particle interactions, with implications for particle energization processes over different spatial scales.

In the previous analysis, we assumed h = 0.05 $\mathrm{R_{Sun}}$. To deepen our understanding of the nuanced behavior of $\mathrm{v_{res\perp}/v_A}$ of particles, we considered h = 0.1 $\mathrm{R_{Sun}}$ for different values of $\mathrm{T_e/T_i}$ and Λ. Our findings reveal that while the resonance velocity maintains a consistent decay rate, we also see a significant change in the normalized distance over which the particles transport energy as illustrated in Fig. 6. Intriguingly, the particles are now imparting acceleration to heat the corona over a short distance in comparison to the scenario with h = 0.05 $\mathrm{R_{Sun}}$; for instance, see Figs. 5 and 6. This signifies that at h = 0.1 $\mathrm{R_{Sun}}$, which is located farther from the Sun, particles in that region can transport energy over a shorter distance compared to h = 0.05 $\mathrm{R_{Sun}}$, which is closer to the Sun. In essence, proximity to the Sun allows particles to transport energy over larger distances ($\mathrm{R_{Sun}}$).

Simultaneously, we unravel the intricate interplay between weak and strong magnetic fields (**B** = 10 G and **B** = 20 G) as a decisive factor influencing the particles' resonance speed. Analogous to the effect of temperature, the magnetic field strength assumes a pivotal role in modulating the particle's resonance characteristics, thereby determining whether they heat the solar corona over larger or shorter distances. This multifaceted analysis highlights the dynamic synergy between height, temperature, and magnetic field strength in shaping the spatial dynamics of wave-particle interactions in the solar coronal environment.

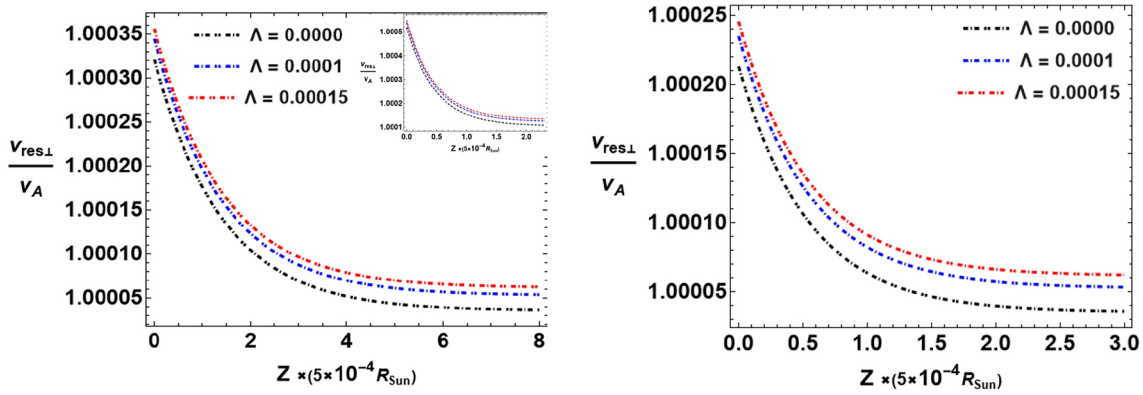

Fig. 5. Normalized perpendicular resonance velocity $\mathrm{v_{res\perp}/v_A}$ vs. normalized distance $Z \times 0.0005\ \mathrm{R_{Sun}}$ for different Λ at fixed $\mathrm{T_e/T_i} = 0.1$. The parameters are the same as those in Fig. 3. In the left panel, we assumed **B** = 10 G, and in the right panel, we assumed **B** = 20 G. The inset is for a larger temperature value of $\mathrm{T_e/T_i} = 0.3$. The perpendicular resonance velocity is significantly influenced by Λ and the electron-to-ion temperature.

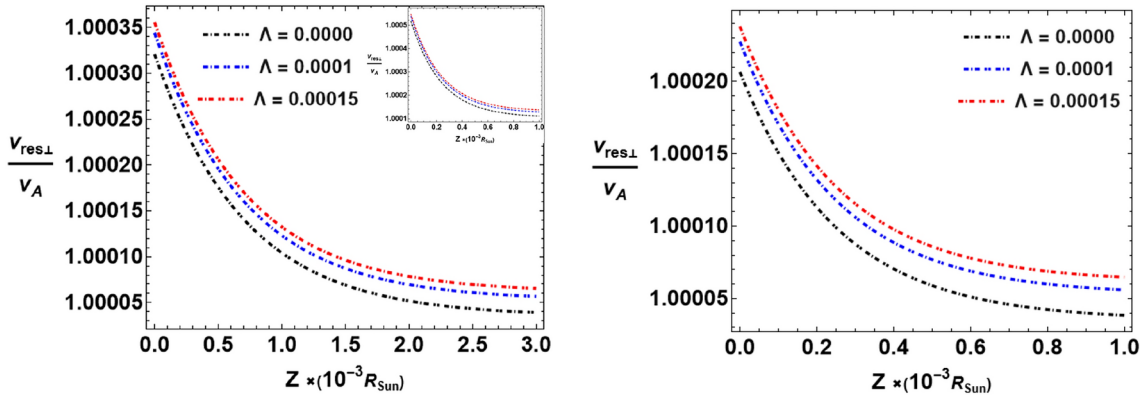

Fig. 6. Normalized perpendicular resonance velocity $\mathrm{v_{res\perp}/v_A}$ vs. normalized distance $Z \times 0.001\ \mathrm{R_{Sun}}$. Here we assumed $\mathrm{h} = 0.1\ \mathrm{R_{Sun}}$ and the other parameters are the same as those in Fig. 3. In the left panel, **B** = 10 G, and in the right panel **B** = 20 G. The inset in the left panel is for a larger temperature ratio$(\mathrm{T_e/T_i} = 0.3)$. Different values of Λ, magnetic field, and temperature significantly influence the resonance velocity.

The physical exploration of the aforementioned analysis on the resultant resonance speed of the particles could be attributed to the nature of the distribution function. The focus of this specific research is on the kinetic limits of Alfvén waves (KAWs), especially concerning ion dynamics. When considering KAWs, the ion dynamics shift the resonance point toward the tail of the electron distribution, as highlighted in Lysak and Lotko[67]. In the tails, we can analyze the slope of the distribution: a positive slope indicates wave growth (instability), while a negative slope signifies wave damping. The sign of the slope is crucial for determining whether the wave will grow or dampen. In Fig. 1 (right panel), for the given values of Λ, the distribution function does not show a positive slope at the resonance points, which are shifted toward the tail due to ion dynamics. Therefore, in our study, the slope is constantly negative, indicating that the wave is damped and gives energy to the particles. We also examined a range of $\Lambda > 1$ values and found that no significant changes occur in the tail of the distribution function, where the resonance points are most relevant. For clarity, we restrict ourselves, not necessarily strictly to follow, the non-thermal parameter Λ to values of $1 \leq \Lambda \geq 0$. This range is also considered in other studies, for example, Bahache et al.[81] studied energetic electrons produced by laser-plasma interactions using the Cairns distribution and found that it is appropriate only for $\Lambda < 0.25$. Other studies also restrict the index parameter to $\Lambda \leq 1$.

On the other hand, it is possible that positive slopes could emerge for $\Lambda > 1$ as can be seen in the expression of the distribution function, but there are constraints on the allowable range of Λ. The possibility of a positive slope in the Cairns distribution could indicate instability. But, in our study, for the values of Λ chosen in the paper, the distribution function does not show a positive slope at the resonance points of KAWs, which are shifted toward the tail due to ion dynamics, as discussed above.

As it is clear from the above discussion, KAWs damped and gave their energy to the particles, the particles can accelerate, gaining a net resonance speed $\mathrm{v_{res}}$. In Fig. 6, based on Eq. (15), it is evident that the changes in

the perpendicular resonance velocity ($v_{res\perp}$) of the particles are not solely influenced by the $C_0 = \left(\frac{1+\frac{\Lambda}{4}}{1+\frac{15\Lambda}{4}}\right)^{1/2}$ term. Upon closer inspection of equation (15), we observe significant contributions from the E_z/E_x and γ terms, as outlined in Eqs. (8) and (9). Additionally, the non-thermal index parameter Λ plays a critical role in these expressions, further impacting the magnitude and distance over which the particles transport energy and heat the surrounding corona. The pronounced sensitivity can also be attributed to Λ in the E_z/E_x and γ.

Figure. 7 provides a comprehensive illustration of the interdependence between the normalized group velocity v_g/v_A as a function of the normalized perpendicular wavenumber $k_x\rho_i$ for different values of Λ . The group velocity of KAWs is substantially influenced by the interplay between Λ and $k_x\rho_i$. The focus of this paper is KAWs in the solar corona, the increase in the magnitude of the group velocity with higher non-thermal parameter Λ or the normalized perpendicular wavenumber $k_x\rho_i$ indicates a highly energetic plasma environment. The larger Λ values suggest a greater presence of energetic particles, enhancing wave-particle interactions and energy transfer, leading to increased group velocity of KAWs. Similarly, an increase in $k_x\rho_i$ denotes shorter wavenumber waves carrying more energy and experiencing stronger magnetic tension which accelerates particles more effectively. This dynamic interplay enhances the propagation characteristics of KAWs, contributing to coronal heating and efficient particle acceleration, and thus plays a crucial role in understanding the solar corona's energetic processes.

Furthermore, we also evaluated the group velocity for different temperature values. We find that the electron-to-ion temperature ratio (T_e/T_i) minimally influences the group velocity. This observation stems from the mathematical expression Eq. (18) governing the group velocity, where the temperature term contributes similarly. The equilibrium in the temperature ratio's impact implies that variations in T_e/T_i do not significantly alter the normalized group velocity of KAWs.

Figure. 8 illustrates the variation in the characteristic damping length L_D of KAWs as a function of $k_x\rho_i$ for $\Lambda \geq 0$. Notably, KAWs exhibit an accelerated damping rate in Cairns-distributed plasmas, reaching resonance at a higher $k_x\rho_i$ value (i.e., ~ 0.06) where the curves for different distributions converge. Beyond this point, no discernible difference between a Cairns and a Maxwellian plasma is observed. The amplitude of L_D reduces with increasing values of the nonthermal parameter Λ. Additionally, under a magnetic field strength of $\mathbf{B} = 20$ G (right panel), the magnitude of damping length experiences a further reduction.

In a broader context, the magnetic field strength plays a pivotal role in shaping the resonance interactions and dispersion characteristics of KAWs. The magnetic field defines the Alfvén speed v_A, influencing the wave-particle resonance conditions. The resonance occurs when the wave frequency aligns with the cyclotron frequency of plasma particles. In a strong magnetic field ($\mathbf{B} = 20$ G), resonance conditions become more restrictive, limiting the effective interaction range of particles with the wave. This, in turn, results in steeper dispersion relations for KAWs, distributing the wave energy over a smaller range of the normalized perpendicular wavenumber $k_x\rho_i$. Although this leads to shorter damping lengths, signifying a rapid decay over a shorter spatial distance, it highlights the sensitivity of KAWs to magnetic field strength.

Conversely, in a weak magnetic field of $\mathbf{B} = 10$ G (left panel), a broader range of resonance particles is facilitated, resulting in longer damping lengths and slower decay of wave energy over a larger spatial distance. Notably, these observations hold consistently with an electron-to-ion temperature ratio of 0.1. Importantly, the **B**-field strength in this specific analysis distinctly affects the magnitude of L_D while leaving $k_x\rho_i$ relatively unaffected. This underscores the intricate coupling of $k_x\rho_i$ and plasma conditions, emphasizing its resilience to variations in magnetic field strength.

When the electron-to-ion temperature ratio is elevated to $T_e/T_i = 0.3$, as shown in Fig. 9, a notable reduction in the magnitude of the damping length occurs. Compared to the previous situation when $T_e/T_i = 0.1$, we see

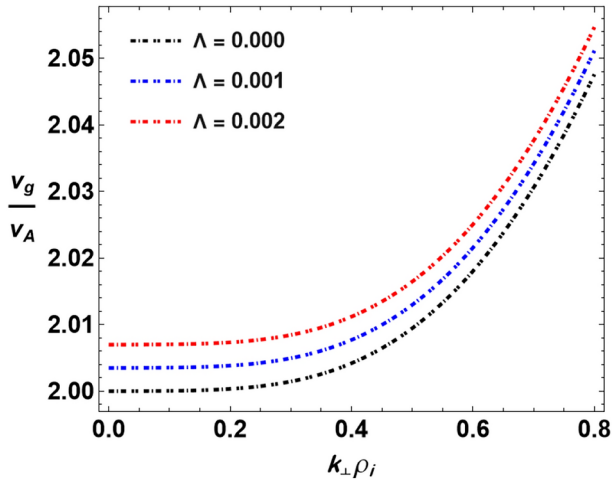

Fig. 7. Normalized group velocity v_g/v_A vs. normalized perpendicular wavenumber $k_x\rho_i$ for different values of Λ with the same parameter values used in Fig. 3. Different values of the index $\Lambda \geq 0$ increase the magnitude of v_g/v_A.

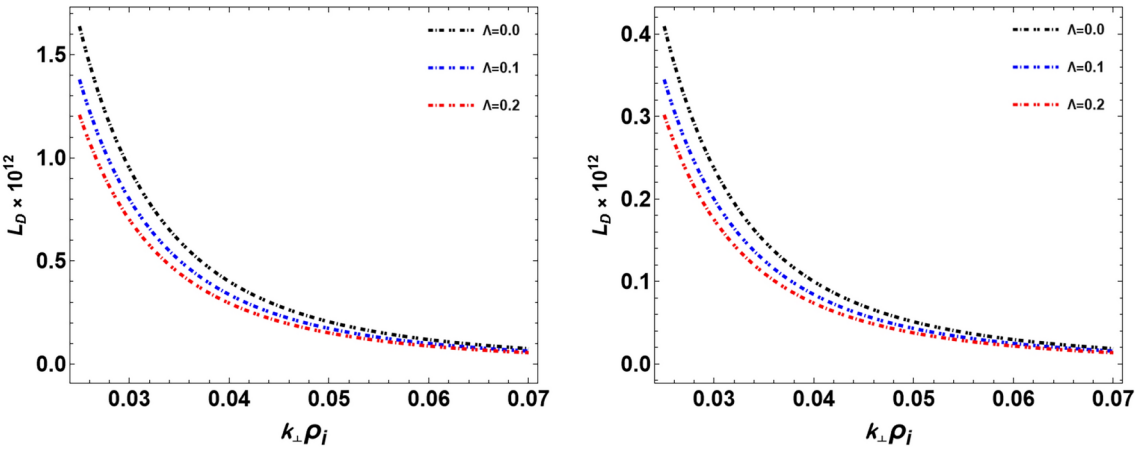

Fig. 8. The characteristic damping length $\mathrm{L_D}$ vs. normalized perpendicular wavenumber $k_x\rho_i$ for different values of Λ at a constant temperature ratio $\mathrm{T_e/T_i} = 0.1$. The plots are based on Eq. (19) with the same parameter values as those which we assumed in Fig. 3. In the left panel, **B** = 10 G, and in the right panel, **B** = 20 G. The damping length is significantly influenced by different values of Λ.

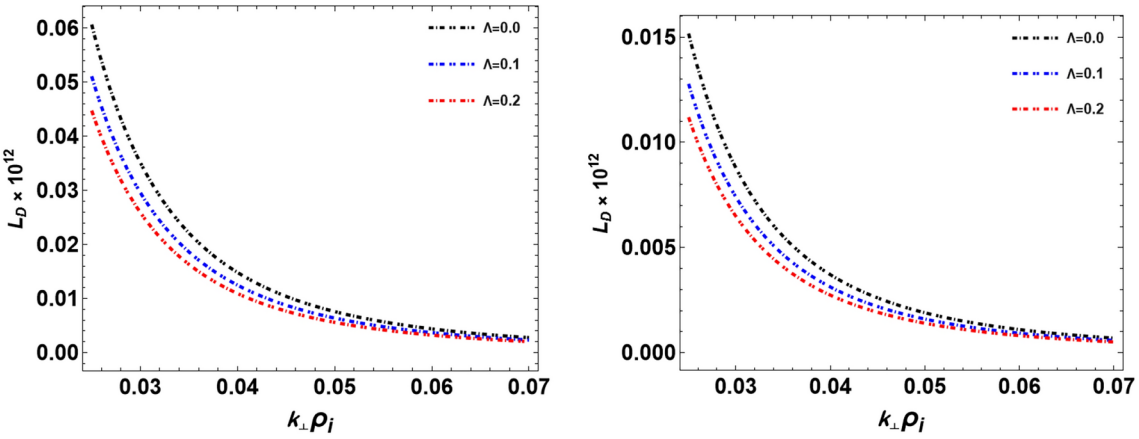

Fig. 9. The characteristic damping length $\mathrm{L_D}$ vs. $k_x\rho_i$ for different values of Λ at constant temperature ratio $\mathrm{T_e/T_i} = 0.3$. The figures show that the magnitude of the damping length is further reduced for $\Lambda > 0$ and $\mathrm{T_e/T_i} = 0.3$. In the left panel, we assumed **B** = 10 G, and in the right panel, we assumed **B** = 20 G.

that the normalized perpendicular wavenumber $k_x\rho_i$ remains the same, implying that the large temperature values do not affect the distance over which the waves transform energy. However, the temperature ratio predominantly influences the magnitude of the damping length, exerting minimal impact on the distance the wave can effectively heat the plasma. Furthermore, the wave exhibits a swifter damping length for $\Lambda \geq 0$, aligning with expectations outlined in the introduction and substantiated by prior works[19,20].

During resonance conditions, the presence of non-thermal particles, characterized by Λ, exerts a substantial influence on the energy transfer dynamics of KAWs within the coronal plasma. This investigation is consistent with the comprehensive analysis provided by Khan et al.[9], offering a detailed analysis of the heating phenomena associated with Alfvén waves in the solar corona.

Concluding remarks

In this work, we utilized the Cairns-distribution function within the conventional Vlasov-Maxwell system, navigating the intricacies of kinetic plasma theory to address in detail the role of KAWs and charged particles heating in the solar corona and solar wind regions. Drawing insights from our earlier exploration of the Poynting flux vector, we conducted an in-depth investigation on the resonance speed, the group velocity, and the characteristic damping length of KAWs, leading to the following key conclusions:

1. Resonance velocity dynamics: The resonance velocity experiences a slow decay within a Cairns-distributed plasma, concurrently heating particles across an extended spatial realm. We evaluated the net resonance velocity in both the parallel and perpendicular directions. The influence of the magnetic field strength is an important factor, diminishing both the magnitude and the corresponding transport distance traveled by the

resonance particles. Physically, this signifies that in a strong magnetic field, robust wave-particle interactions lead to resonance over shorter distances, whereas a weaker magnetic field allows the particles to traverse larger distances (R_{Sun}).

2. Parallel vs. perpendicular heating: KAWs predominantly carry energy in the direction parallel to the ambient magnetic field due to the condition $k_\perp \gg k_\parallel$. This is evident in the expressions of the Poynting flux vectors, thoroughly discussed in our recent work[28]. Our research focuses on KAWs within the solar wind and solar corona, particularly the solar flux tube loops. In the loops, parallel heating occurs along the height, while perpendicular heating occurs along the width, forming a semi-circular loop. KAWs are more rapidly damped in the perpendicular direction, thus carrying less energy. This observation aligns with Leamon et al.[82], which demonstrates that in coronal conditions, perpendicular cascades lead to faster energy dissipation at small scales compared to linear proton cyclotron dissipation. In our study, as shown in Figs. 5 and 6, the resonance velocity in the perpendicular direction significantly decays at a faster rate over a short distance (R_{Sun}), indicating less energy transfer and heating. Zank et al.[36] investigated the heating of core solar coronal protons using a turbulence transport model, finding that strong perpendicular heating occurs within the range of $(0-3)R_{Sun}$. This highlights the distinct heating mechanisms at play within the solar corona and emphasizes the importance of understanding both parallel and perpendicular heating in solar plasma dynamics.
3. Group velocity: The nuanced interplay of Λ values yields an enhanced group velocity in Cairns-distributed plasma compared to a Maxwellian counterpart. However, an increase in the temperature (T_e/T_i) ratio does not significantly influence the group velocity of KAWs.
4. Damping length: The characteristic damping length is reduced with increasing the Cairns parameter Λ. A strong magnetic field manifested in a decreased damping length magnitude, although, the magnetic field does not alter the normalized distance characterizzed by $k_x\rho_i$. Furthermore, increasing the electron-to-ion temperature ratio (i.e., 0.3) exacerbated this effect, emphasizing that the combined influence of magnetic field strength and increased temperature ratio results in a reduced damping length. This phenomenon signifies rapid damping length, with the wave relinquishing its energy to particles over a short distance.Future extensions of this work could include the effects of energetic particles and temperature anisotropies using a Cairns distribution. This approach would help us understand how these factors influence KAW properties, particularly in converting wave energy to particle heating both perpendicular and parallel to the mean magnetic field.

Data availibility

All data generated or analyzed during this study are included in this published article. The work consists of detailed theoretical derivations, which will be made available (in step-wise form) upon reasonable request. For data inquiries, don't hesitate to contact the corresponding author, S. Ayaz.

Received: 24 July 2024; Accepted: 28 October 2024
Published online: 14 November 2024

References

1. Parker, E. N. Dynamics of the interplanetary gas and magnetic fields. *Astrophys. J.* **128**, 664 (1958).
2. Parker, E. N. Interplanetary dynamical processes. *New York* (1963).
3. Hughes, R. S., Gary, S. P., Wang, J. & Parashar, T. N. Kinetic alfvén turbulence: Electron and ion heating by particle-in-cell simulations. *Astrophys. J. Lett.* **847**, L14 (2017).
4. Marsch, E. Solar wind and kinetic heliophysics. *Annales Geophysicae* **36**, 1607–1630 (2018).
5. Alfvén, H. Existence of electromagnetic-hydrodynamic waves. *Nature* **150**, 405–406 (1942).
6. Wang, B.-B., Zank, G. P., Adhikari, L. & Zhao, L.-L. On the conservation of turbulence energy in turbulence transport models. *Astrophys. J.* **928**, 176 (2022).
7. Gershman, D. J. et al. Wave-particle energy exchange directly observed in a kinetic alfvén-branch wave. *Nat. Commun.* **8**, 14719 (2017).
8. Hasegawa, A. & Chen, L. Kinetic processes in plasma heating by resonant mode conversion of alfvén wave. Tech. Rep., Princeton Plasma Physics Lab.(PPPL), Princeton, NJ (United States) (1976).
9. Khan, I. A., Iqbal, Z. & Murtaza, G. Solar coronal heating by alfvén waves in bi-kappa distributed plasma. *Mon. Not. R. Astron. Soc.* **491**, 2403–2412 (2020).
10. Salem, C. S. et al. Identification of kinetic alfvén wave turbulence in the solar wind. *Astrophys. J. Lett.* **745**, L9 (2012).
11. Chen, L., Zonca, F. & Lin, Y. Physics of kinetic alfvén waves: A gyrokinetic theory approach. *Rev. Modern Plasma Phys.* **5**, 1–37 (2021).
12. Rivera, Y. J. et al. In situ observations of large-amplitude alfvén waves heating and accelerating the solar wind. *Science* **385**, 962–966 (2024).
13. Chaston, C. *et al.* Properties of small-scale alfvén waves and accelerated electrons from fast. *J. Geophys. Res. Space Phys.***108** (2003).
14. Keiling, A., Wygant, J., Cattell, C., Mozer, F. & Russell, C. The global morphology of wave poynting flux: Powering the aurora. *Science* **299**, 383–386 (2003).
15. Chaston, C. C., Bonnell, J., Reeves, G. D. & Skoug, R. Driving ionospheric outflows and magnetospheric o+ energy density with alfvén waves. *Geophys. Res. Lett.* **43**, 4825–4833 (2016).
16. Boldyrev, S. & Perez, J. C. Spectrum of kinetic-alfvén turbulence. *Astrophys. J. Lett.* **758**, L44 (2012).
17. Liu, Z.-Y. et al. Particle-sounding of the spatial structure of kinetic alfvén waves. *Nat. Commun.* **14**, 2088 (2023).
18. Temerin, M., Kletzing, C. A., Scudder, J. & Streltsov, A. V. Evidence for kinetic alfvén waves and parallel electron energization at 4–6 re altitudes in the plasma sheet boundary layer. *J. Geophys. Res.* **107**, 2002 (2001).
19. Lee, L., Johnson, J. R. & Ma, Z. Kinetic alfvén waves as a source of plasma transport at the dayside magnetopause. *J. Geophys. Res. Space Phys.* **99**, 17405–17411 (1994).
20. Shukla, N., Varma, P. & Tiwari, M. Study on kinetic alfven wave in inertial regime. *Indian J. Pure Appl. Phys.* (2009).
21. Wu, D.-J. & Chen, L. *Kinetic Alfvén waves in laboratory, space, and astrophysical plasmas* (Springer, 2020).
22. Louarn, P. et al. Observation of kinetic alfvén waves by the freja spacecraft. *Geophys. Res. Lett.* **21**, 1847–1850 (1994).
23. Chaston, C. et al. The turbulent alfvénic aurora. *Phys. Rev. Lett.* **100**, 175003 (2008).

24. Sahraoui, F., Goldstein, M., Robert, P. & Khotyaintsev, Y. V. Evidence of a cascade and dissipation of solar-wind turbulence at the electron gyroscale. *Phys. Rev. Lett.* **102**, 231102 (2009).
25. Alexandrova, O., Lacombe, C., Mangeney, A., Grappin, R. & Maksimovic, M. Solar wind turbulent spectrum at plasma kinetic scales. *Astrophys. J.* **760**, 121 (2012).
26. Chen, C., Klein, K. & Howes, G. G. Evidence for electron landau damping in space plasma turbulence. *Nat. Commun.* **10**, 740 (2019).
27. Parashar, T. N. et al. Turbulent dissipation challenge: A community-driven effort. *J. Plasma Phys.* **81**, 905810513 (2015).
28. Ayaz, S., Li, G. & Khan, I. A. Solar coronal heating by kinetic alfvén waves. *Astrophys. J.* **970**, 140. https://doi.org/10.3847/1538-4357/ad5bdc (2024).
29. Fahr, H. & Shizgal, B. Modern exospheric theories and their observational relevance. *Rev. Geophys.* **21**, 75–124 (1983).
30. Schwenn, R. Large-scale structure of the interplanetary medium. *Physics of the inner heliosphere I: large-scale phenomena* 99–181 (1990).
31. Marsch, E. Kinetic physics of the solar corona and solar wind. *Living Rev. Sol. Phys.* **3**, 1–100 (2006).
32. Benz, A. O. *Plasma Astrophysics: Kinetic Processes in Solar and Stellar Coronae* Vol. 184 (Springer Science & Business Media, 2012).
33. Aschwanden, M. J. & Aschwanden, M. J. *Particle Acceleration and Kinematics in Solar Flares: A Synthesis of Recent Observations and Theoretical Concepts (Invited Review)* (Springer, 2002).
34. Aschwanden, M. *Physics of the Solar Corona: An Introduction with Problems and Solutions* (Springer Science & Business Media, 2006).
35. Matthaeus, W. H., Zank, G. P., Smith, C. W. & Oughton, S. Turbulence, spatial transport, and heating of the solar wind. *Phys. Rev. Lett.* **82**, 3444 (1999).
36. Zank, G. et al. Theory and transport of nearly incompressible magnetohydrodynamic turbulence. IV. Solar coronal turbulence. *Astrophys. J.* **854**, 32 (2018).
37. Zank, G. *et al.* Turbulence transport in the solar corona: Theory, modeling, and parker solar probe. *Phys. Plasmas***28** (2021).
38. Hollweg, J. V. Kinetic alfvén wave revisited. *J. Geophys. Res. Space Phys.* **104**, 14811–14819 (1999).
39. Pezzi, O. et al. Turbulence generation during the head-on collision of alfvénic wave packets. *Phys. Rev. E* **96**, 023201 (2017).
40. Bale, S. D., Kellogg, P., Mozer, F., Horbury, T. & Reme, H. Measurement of the electric fluctuation spectrum of magnetohydrodynamic turbulence. *Phys. Rev. Lett.* **94**, 215002 (2005).
41. Bale, S. et al. Highly structured slow solar wind emerging from an equatorial coronal hole. *Nature* **576**, 237–242 (2019).
42. Kasper, J. C. et al. Alfvénic velocity spikes and rotational flows in the near-sun solar wind. *Nature* **576**, 228–231 (2019).
43. Vranjes, J. & Poedts, S. Kinetic instability of drift-alfvén waves in solar corona and stochastic heating. *Astrophys. J.* **719**, 1335 (2010).
44. Liu, Y., Liu, S., Dai, B. & Xue, T. Dispersion and damping rates of dispersive alfvén wave in a nonextensive plasma. *Phys. Plasmas***21** (2014).
45. Rubab, N., Ali, S. & Jaffer, G. Dust kinetic alfvén waves and streaming instability in a non-maxwellian magnetoplasma. *Phys. Plasmas***21** (2014).
46. Huo, R., Du, J. & Guo, R. Kinetic alfvén waves in the temperature anisotropic space plasma with a kappa-maxwellian distribution. *Chin. J. Phys.* **90**, 199–208 (2024).
47. Cairns, R. et al. Electrostatic solitary structures in non-thermal plasmas. *Geophys. Res. Lett.* **22**, 2709–2712 (1995).
48. Bostrom, R. Observations of weak double layers on auroral field lines. *IEEE Trans. Plasma Sci.* **20**, 756–763 (1992).
49. Dovner, P., Eriksson, A., Boström, R. & Holback, B. Freja multiprobe observations of electrostatic solitary structures. *Geophys. Res. Lett.* **21**, 1827–1830 (1994).
50. Summers, D. & Thorne, R. M. The modified plasma dispersion function. *Phys. Fluids B* **3**, 1835–1847 (1991).
51. Zank, G. Formation of kappa distributions at quasiperpendicular shock waves. In *Kappa Distributions* (ed. Zank, G.) 609–632 (Elsevier, 2017).
52. Zank, G., Heerikhuisen, J., Pogorelov, N., Burrows, R. & McComas, D. Microstructure of the heliospheric termination shock: Implications for energetic neutral atom observations. *Astrophys. J.* **708**, 1092 (2009).
53. Yang, Z. et al. Impact of pickup ions on the shock front nonstationarity and energy dissipation of the heliospheric termination shock: Two-dimensional full particle simulations and comparison with voyager 2 observations. *Astrophys. J.* **809**, 28 (2015).
54. Mamun, A. Rarefactive ion-acoustic electrostatic solitary structures in nonthermal plasmas. *Eur. Phys. J. D-Atom. Mol. Opt. Plasma Phys.* **11**, 143–147 (2000).
55. Jukui, X. Modulational instability of ion-acoustic waves in a plasma consisting of warm ions and non-thermal electrons. *Chaos Solitons Fractals* **18**, 849–853 (2003).
56. Verheest, F. & Hellberg, M. A. Compressive and rarefactive solitary waves in nonthermal two-component plasmas. *Phys. Plasmas***17** (2010).
57. Baluku, T. & Hellberg, M. Ion acoustic solitary waves in an electron-positron-ion plasma with non-thermal electrons. *Plasma Phys. Controlled Fusion* **53**, 095007 (2011).
58. Rehman, A. U., Shahzad, M. A., Mahmood, S. & Bilal, M. Numerical and analytical study of electron plasma waves in nonthermal vasyliunas-cairns distributed plasmas. *J. Geophys. Res. Space Phys.* **126**, e2021JA029626 (2021).
59. Fitzenreiter, R. J., Klimas, A. J. & Scudder, J. D. Detection of bump-on-tail reduced electron velocity distributions at the electron foreshock boundary. *Geophys. Res. Lett.* **11**, 496–499 (1984).
60. Hau, L.-N. & Fu, W.-Z. Mathematical and physical aspects of kappa velocity distribution. *Phys. Plasmas***14** (2007).
61. Wang, B. & Hau, L. General formulation for electrostatic solitons in multicomponent nonthermal plasmas. *Plasma Phys. Controlled Fusion* **57**, 095012 (2015).
62. Retterer, J. M., Chang, T. & Jasperse, J. Ion acceleration by lower hybrid waves in the suprauroral region. *J. Geophys. Res. Space Physics* **91**, 1609–1618 (1986).
63. Livadiotis, G. et al. Pick-up ion distributions and their influence on energetic neutral atom spectral curvature. *Astrophys. J.* **751**, 64 (2012).
64. Möbius, E. et al. Direct observation of he+ pick-up ions of interstellar origin in the solar wind. *Nature* **318**, 426–429 (1985).
65. Khan, I. A., Iqbal, Z., Naim, H. & Murtaza, G. Obliquely propagating magnetosonic waves in a plasma modeled by bi-anisotropic cairns distribution. *Phys. Plasmas***25** (2018).
66. Zank, G. P. *Transport Processes in Space Physics and Astrophysics* Vol. 877 (Springer, 2014).
67. Lysak, R. L. & Lotko, W. On the kinetic dispersion relation for shear alfvén waves. *J. Geophys. Res. Space Phys.* **101**, 5085–5094 (1996).
68. Lysak, R. L. The relationship between electrostatic shocks and kinetic alfvén waves. *Geophys. Res. Lett.* **25**, 2089–2092 (1998).
69. Ayaz, S., Khan, I. A. & Murtaza, G. On the dispersion and damping of kinetic and inertial alfvén waves in cairns distributed plasmas. *Phys. Plasmas***26** (2019).
70. Ayaz, S., Khan, I. A., Iqbal, Z. & Murtaza, G. Alfvén waves in temperature anisotropic cairns distributed plasma. *Commun. Theor. Phys.* **72**, 035502 (2020).
71. Fried, B. D. & Conte, S. D. *The Plasma Dispersion Function: The Hilbert Transform of the Gaussian* (Academic press, 2015).
72. Paraschiv, A., Bemporad, A. & Sterling, A. Physical properties of solar polar jets-a statistical study with hinode xrt data. *Astron. Astrophys.* **579**, A96 (2015).

73. Tiwari, B., Mishra, R., Varma, P. & Tiwari, M. Shear-driven kinetic alfven wave in the plasma sheet boundary layer. *Earth Planets Space* **60**, 191–205 (2008).
74. Zirin, H. The mystery of the chromosphere. *Sol. Phys.* **169**, 313–326 (1996).
75. Gary, G. A. Plasma beta above a solar active region: Rethinking the paradigm. *Sol. Phys.* **203**, 71–86 (2001).
76. Chen, L. & Wu, D. Kinetic alfvén wave instability driven by field-aligned currents in solar coronal loops. *Astrophys. J.* **754**, 123 (2012).
77. Singh, H. D. & Jatav, B. S. Anisotropic turbulence of kinetic alfvén waves and heating in solar corona. *Res. Astron. Astrophys.* **19**, 185 (2019).
78. Li, G. et al. Modeling solar energetic neutral atoms from solar flares and cme-driven shocks. *Astrophys. J.* **944**, 196 (2023).
79. Lysak, R. L. & Song, Y. Kinetic theory of the alfvén wave acceleration of auroral electrons. *J. Geophys. Rese. Space Phys.***108** (2003).
80. Khan, I. A., Iqbal, Z. & Murtaza, G. Perturbed electromagnetic field and poynting flux of kinetic alfvén waves in kappa distributed space plasmas. *Eur. Phys. J. Plus* **134**, 80 (2019).
81. Bahache, A., Bennaceur-Doumaz, D. & Djebli, M. Effects of energetic electrons on ion acceleration in a quasi-static model. *Phys. Plasmas***24** (2017).
82. Leamon, R. J. et al. Mhd-driven kinetic dissipation in the solar wind and corona. *Astrophys. J.* **537**, 1054 (2000).

Acknowledgements

SA acknowledges the support of an NSF grant 2149771 and GPZ the partial support of a NASA Parker Solar Probe contract SV4 - 84017 and an NSF EPSCoR RII - Track - 1 Cooperative Agreement OIA - 2148653.

Author contributions

SA led the investigation into kinetic Alfvén waves (KAWs) in the solar coronal region, with a particular focus on the heating and acceleration of charged particles. Using the kinetic plasma theory approach and a novel Cairns distribution function, SA calculated the resonance speed of particles following wave-particle interactions and the damping length of KAWs. GPZ, SA's current advisor, played an instrumental role in this research. He provided extensive guidance and made several critical suggestions, particularly regarding the choice of the Cairns distribution and the investigation of the perpendicular resonance velocity, which offers new insights into turbulence phenomena. GPZ meticulously reviewed the manuscript, ensuring that each word was precise and the overall quality was exceptional. His expertise and insights significantly enhanced the robustness and clarity of the study. IAK., a key collaborator, verified all analytical results and mathematical equations for accuracy. He introduced the concept of resonance velocity and diligently checked each mathematical step, ensuring the resultant equations were error-free. GL, SA's former advisor, offered initial encouragement and validation for the research idea. He reviewed the draft, verified mathematical equations, and helped in selecting specific parameter values relevant to the solar coronal region, contributing to the development of the graphs and overall study. YJR contributed by providing crucial observational data from the PSP and Solar Orbiter, facilitating the comparison of our analytical findings with real spacecraft measurements. Additionally, YJR played a key role in addressing the referee(s)' questions, ensuring that the observational data aligned seamlessly with the theoretical analysis for a more coherent and consistent interpretation. All authors' combined efforts and contributions have significantly enriched this research, providing a comprehensive and insightful analysis of KAWs in the solar corona.

Declarations

Competing interests

The authors declare no competing interests.

Additional information

Correspondence and requests for materials should be addressed to S.A.

Reprints and permissions information is available at www.nature.com/reprints.

Publisher's note Springer Nature remains neutral with regard to jurisdictional claims in published maps and institutional affiliations.